Journal of Zhejiang University-SCIENCE B (Biomedicine & Biotechnology)
ISSN 1673-1581 (Print); ISSN 1862-1783 (Online)
www.zju.edu.cn/jzus; www.springerlink.com
E-mail: jzus@zju.edu.cn

Simulation of biatrial conduction via different pathways during sinus rhythm with a detailed human atrial model*

Dong-dong DENG[1], Ying-lan GONG[1], Guo-fa SHOU[1], Pei-feng JIAO[2], Heng-gui ZHANG[3], Xue-song YE[1], Ling XIA[†‡1]

([1]*College of Biomedical Engineering and Instrument Science, Zhejiang University, Hangzhou 310027, China*)

([2]*Institute of Clinical Anatomy, Southern Medical University, Guangzhou 510515, China*)

([3]*Biological Physics, University of Manchester, Manchester M13 9PL, UK*)

[†]E-mail: xialing@zju.edu.cn

Received Nov. 4, 2011; Revision accepted Feb. 28, 2012; Crosschecked Aug. 9, 2012

Abstract: In order to better understand biatrial conduction, investigate various conduction pathways, and compare the differences between isotropic and anisotropic conductions in human atria, we present a simulation study of biatrial conduction with known/assumed conduction pathways using a recently developed human atrial model. In addition to known pathways: (1) Bachmann's bundle (BB), (2) limbus of fossa ovalis (LFO), and (3) coronary sinus (CS), we also hypothesize that there exist two fast conduction bundles that connect the crista terminalis (CT), LFO, and CS. Our simulation demonstrates that use of these fast conduction bundles results in a conduction pattern consistent with experimental data. The comparison of isotropic and anisotropoic conductions in the BB case showed that the atrial working muscles had small effect on conduction time and conduction speed, although the conductivities assigned in anisotropic conduction were two to four times higher than the isotropic conduction. In conclusion, we suggest that the hypothesized intercaval bundles play a significant role in the biatrial conduction and that myofiber orientation has larger effects on the conduction system than the atrial working muscles. This study presents readers with new insights into human atrial conduction.

Key words: Cardiac electrophysiology, Conduction, Human atrial model, Modeling
doi:10.1631/jzus.B1100339 **Document code:** A **CLC number:** R541.7+3; Q25; Q46

1 Introduction

Biatrial conduction during sinus rhythm (SR) has been widely studied (Anderson *et al*., 1979; Boineau *et al*., 1988; Bromberg *et al*., 1995; Anderson *et al*., 2000; Burashnikov *et al*., 2004; Anderson and Cook, 2007), and the reported conduction pathways can be summarized as Bachmann's bundle (BB), limbus of fossa ovalis (LFO), and coronary sinus (CS) (de Ponti *et al*., 2002; Markides *et al*., 2003; Lemery *et al*., 2004; Jurkko *et al*., 2010). The experimental data showed that the BB is the most prominent pathway, but in pathologic conditions the ratio of BB conduction decreases significantly. Jurkko *et al*. (2010) reported the quantitative measurements of the proportion of conduction pathways in the control and atrial fibrillation (AF) patients, and showed that the ratio of BB conduction decreased from 67% to 54% in AF patients.

The quantitative biatrial conduction via BB has been investigated by many groups (de Ponti *et al*., 2002; Markides *et al*., 2003; Lemery *et al*., 2004; 2007; Jurkko *et al*., 2009; Tapanainen *et al*., 2009), and the results are not significantly different between

‡ Corresponding author

* Project supported by the National Basic Research Program (973) of China (No. 2007CB512100), the National High-Tech R & D Program (863) of China (No. 2006AA02Z307), the National Natural Science Foundation of China (Nos. 81171421 and 61101046), and the Zhejiang Provincial Natural Science Foundation of China (No. Z1080300)

the groups. However, the quantitative biatrial conduction with other pathways like CS, LFO, or their combination has been rarely reported. Recently, magnetocardiography (MCG) has been used to measure the time of biatrial conduction via different pathways, and some novel and interesting results have been presented (Jurkko *et al*., 2009; 2010; Tapanainen *et al*., 2009). Tapanainen *et al*. (2009) reported that when conduction was via BB (either through a single route or as part of combined routes), the total left atrial activation was significantly shorter, and when LFO was involved in the biatrial conduction, the left atrial activation started earlier but the duration of left atrial activation lasted longer. Furthermore, they showed that when CS was the only biatrial conduction pathway, the total atrial activation time was less than that via BB. However, such a phenomenon has not been reproduced by other researchers.

In addition to vast experimental data, many computer models have been used to study biatrial conduction (Harrild and Henriquez, 2000; Zozor *et al*., 2003; Seemann *et al*., 2006); however, the previous simulation study always involved only one or two conduction pathways. Harrild and Henriquez (2000) applied a detailed human atrial anatomy model to simulate atrial excitation conduction, in which the BB and LFO were considered. Seemann *et al*. (2006) used a visible female dataset (Sachse *et al*., 2000) to simulate biatrial conduction, and only the BB was taken into account. Since the experimental data showed that more than one pathway existed in biatrial conduction, and that the conduction patterns may vary when different pathways were involved in biatrial conduction, the model, including only one or two pathways, seems insufficient to study the effect of varied pathways.

New experimental results have shown that when CS or LFO was involved in biatrial conduction, the earliest activation happened in left atrium (LA) and the total left atrial activation time had large differences. To better understand these results and to investigate the effect of different conduction pathways, we present a detailed simulation study of the various conduction pathways in biatrial conduction. In addition to the known pathways: (1) BB, (2) LFO, and (3) CS, we also assumed that there existed two fast conduction bundles that connected the crista terminalis (CT), LFO, and CS, which were reported by the previous anatomic evidence of human heart (Wang *et al*., 1995; Ho *et al*., 2002a). The simulation is carried out using a detailed anatomic biatrial model incorporated with realistic measured fiber orientation. The interesting phenomenon reported by Jurkko (2009) is well explained based on the simulation results. Furthermore, the differences in conduction patterns between isotropic and anisotropic conductions were also compared.

2 Materials and methods

2.1 Cardiome-CN human atrial anatomic model

The heart specimen in this study was collected from a healthy adult male in Zhujiang Hospital, Southern Medical University, China, with approval from the ethics committee at the Southern Medical University and following the Chinese law of heart research. The heart specimen was scanned using spiral computerized tomography (Philips/Brilliance 64, Netherlands). The size is 512 pixels×512 pixels, and the spatial resolution is 0.3574 mm× 0.3574 mm×0.33 mm.

The software ScanIP (Simpleware Inc., Bradninch Hall, UK) was used to segment and reconstruct the heart from the scanned images. Limited by the images' resolution, the fast conduction bundles in the atria cannot be directly obtained from the images, therefore, we used Mimics (Materialize Inc., Leuven, Belgium) to construct the conduction system referred to in the previous publications about human atrial anatomic data (Anderson *et al*., 1979; 2000; James, 2002; Sanchez-Quintana *et al*., 2002; Lemery *et al*., 2003; Hucker *et al*., 2008; Saremi *et al*., 2008; Ho and Sanchez-Quintana, 2009). The detailed method used to obtain and construct the heart model can be found in Deng *et al*. (2012). The final obtained anatomical structure of the Cardiome-CN human atrial heart is displayed in Fig. 1a. The conduction bundles are illustrated in Fig. 1b, and the relative location of the bundles in atria is shown in Fig. 1c.

In this model the sinoatrial node (SAN) includes the center and periphery parts and locates at the superior poster lateral wall of the right atrium

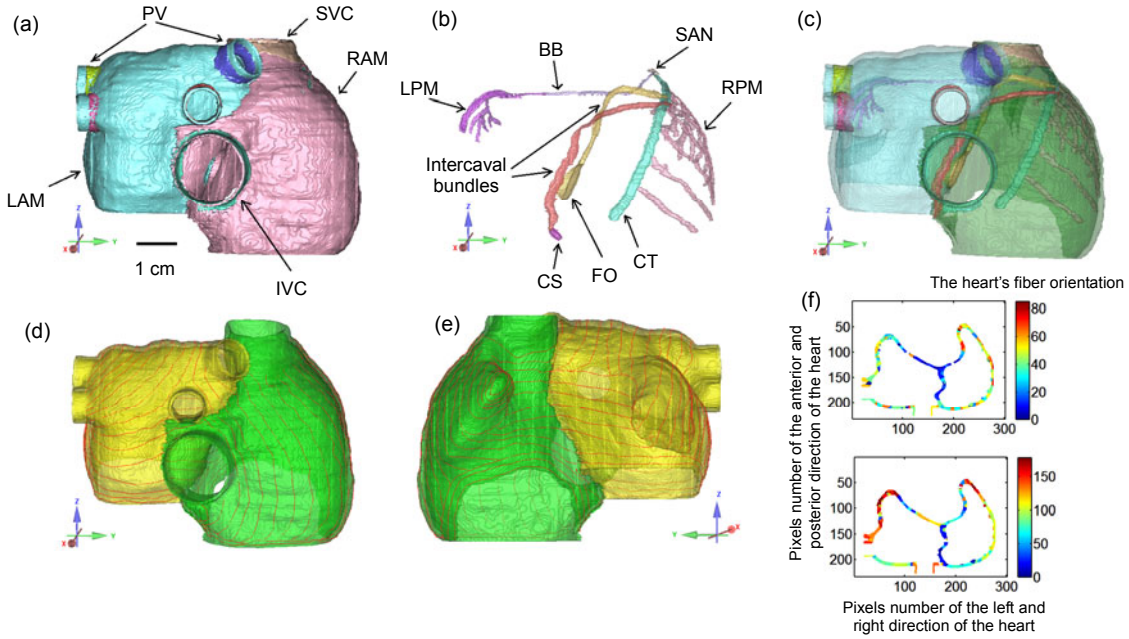

Fig. 1 Anatomical illustration of the Cardiome-CN human atrial model

(a) Posterior view of the atria; (b) Conduction bundles in the atria; (c) Transparent display of the conduction bundles and atrial muscles; (d) Fiber orientation within the atrial anatomic model in the anterior view; (e) Fiber orientation within the atrial anatomic model in the posterior view; (f) The top image represents the inclination angle of one cross section of the atria in (a), the bottom image is the transverse angle of the same cross section. The 3D orientation of the atria in each figure is given in the corner, and the space scale is also listed; the following figures use the same space scale. PV: pulmonary veins; SVC: superior vena cava; IVC: inferior vena cava; LAM: left atrial muscles; RAM: right atrial muscles; LPM: left pectinate muscles; RPM: right pectinate muscles; BB: Bachmann's bundle; SAN: sinoatrial node; CS: coronary sinus; FO: fossa ovalis; CT: crista terminalis

(RA); its size is about 10 mm×4 mm×1 mm which is based on experimental data (Anderson *et al*., 2009; Fedorov *et al*., 2010). There is little quantitative data about CT and pectinate muscles (PM), so in this paper, we used qualitative description of the position and anatomic structure to construct them (Sanchez-Quintana *et al*., 2002; Ho and Sanchez-Quintana, 2009). In our model, consistent with experimental data, the length of the BB is 14.7 mm, the maximum anteroposterior diameter is 4.5 mm, and the maximum superoinferior diameter is 3.7 mm (Lemery *et al*., 2003; Saremi *et al*., 2008). The diameter of the fossa ovalis (FO) is 16 mm, and the shortest distance to the BB is 16 mm, which is a little longer than the experimental data (Lemery *et al*., 2003). The starting position and opening diameter (7.8 mm) of the CS are based on the original images. However, because the site of left atrial insertion cannot be distinguished in the images, we set the distance from CS ostium to left atrium as 10 mm, based on the anatomic data (Chauvin *et al*., 2000; Matsuyama *et al*., 2010). It is worth mentioning that in this model two intercaval bundles are included: the first connects the CT and the antero-superior rim of FO, and the other connects the CT and CS.

In our simulation, the excitation from SAN can conduct to CT, but not atrial muscles, since Fedorov *et al*. (2010) showed that the SAN was functionally insulated from the surrounding atrial myocytes except for a limited number of exit sites. BB can conduct the excitation from RA to LA and it couples with atria only at the two ends, as shown by Harrild and Henriquez (2000). CT and PM can spread to atrial muscles, and vice versa, but the anisotropy is set as 9:1 (Henriquez *et al*., 1996; Harrild and Henriquez, 2000; Seemann *et al*., 2006). The properties of the two intercavel bundles are set as for those of CT and PM.

2.2 Fiber orientation of the atria

Due to the complexity of atrial myoarchitecture, there are few studies that quantitatively describe atria

fiber orientation and only a small number of qualitative anatomical studies are available (Wang *et al*., 1995; Ho *et al*., 1999; 2002a; 2002b; Anderson and Cook, 2007; Ho and Sanchez-Quintana, 2009). In order to obtain the fiber orientation, some atrial muscles were peeled off along the fiber orientation after being scanned by a computerized tomography scanner, and then the heart was scanned by the 3D laser scanner (RealScan USB Scanner model 200, 3D Digital Corporation, USA). Scan spatial resolution is 0.01 mm and the total point of the epicardium is about 0.3 million. Geomagic software (Geomagic Inc., Davis Drive, USA) was used to trace the fiber orientation.

The original data for myocardial fiber orientation was from the 3D laser scanned pictures of the human heart. Because the two layers of data were not obtained at the same coordinate, registration was carried out using the method we previously described (Deng *et al*., 2009). After registration, fiber orientations of endocardia and epicardia were set at the same coordinate allowing the data to be used to construct the whole atrial fiber orientation. Figs. 1d and 1e show all the measured points along with fiber orientation data but they only contain the surface fiber orientation of the atria, and the remaining atrial muscles do not have the fiber orientation, so based on these measured atrial fiber data, the interpolation process was applied to all atrial points as follows. First the fiber data was projected onto the anatomic model, and then the points closest to those with fiber data were identified and assigned corresponding fiber data. For the fiber orientation of fast conduction bundles, we used Mimics software to depict vectors along the principal axis of the conduction system (data not shown), similar to the method used by Seemann *et al*. (2006). Once the fiber orientation of conduction bundles was obtained, fiber orientation of whole atria was completed. In simulation, we used two angles to represent a vector as demonstrated by previous researchers (Rijcken *et al*., 1999; Rohmer *et al*., 2007). Fig. 1f shows the inclination angle and the transverse angle of one cross section of the atria; the color represents the degree of the angle.

2.3 Atrial cell models

The atria include many kinds of cells, which add to the variability of atrial cellular models. The SAN should be set up first, though it is difficult to measure normal human SAN data. Recently, by investigating the expression of ion channels in the human SAN (Chandler *et al*., 2009), a human SAN action potential (AP) model was developed based on the human atrial cell model (Courtemanche *et al*., 1998). Since most of the ionic parameters in the AP model come from experimental data, the electrical properties of SAN are likely to be realistically reflected, thus it was used in our simulation (Fig. 2). In our simulation, the frequency of the autorhythm of central SAN cell is 1.19 Hz, the maximum diastolic potential of the central cell is −50.82 mV, and the overshoot is 12.29 mV. As was demonstrated previously, the peripheral cell does not have autorhythmicity (Chandler *et al*., 2009); its resting potential is −78.37 mV, and the overshoot is 5.77 mV.

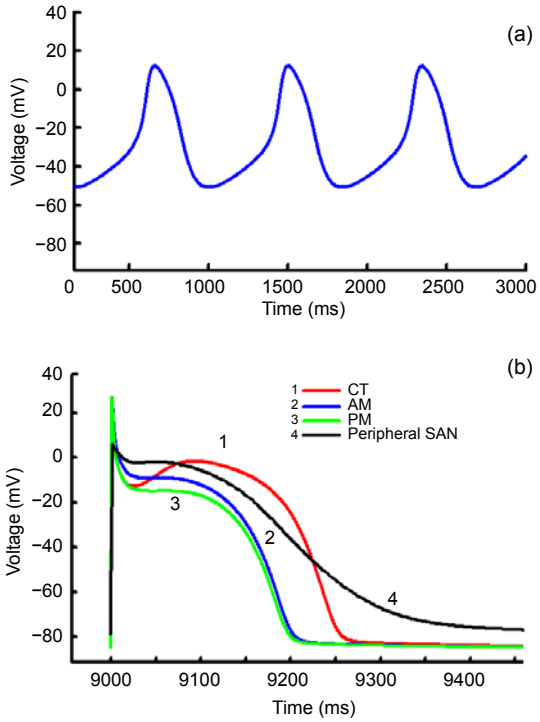

Fig. 2 Action potential (AP) models used in our simulation

(a) AP of central SAN; (b) AP of peripheral SAN, atrial musle (AM), crista terminalis (CT), and pectinate muscles (PM)

Experimental data has shown that the electrophysiological properties of atrial tissue from different anatomical regions of dogs were different (Feng *et al*., 1998; Burashnikov *et al*., 2004). The parameters used in this study to simulate the electrical propagation of

atria were based on those used in previous work (Courtemanche *et al*., 1998; Feng *et al*., 1998; Seemann *et al*., 2006). Although Duytschaever *et al*. (2002) reported that in goat the absolute refractory period at middle part of BB was much longer than that at RA and LA, and Feng *et al*. (1998) descried that the AP duration in CT was longer than that in atrial muscles, the APs of BB and CT were both longer than that in the atrial muscles, and they are both the fast conduction bundles whose conduction speed is much higher than that of the atrial muscles, a cell model of BB has not yet been developed. Therefore, in this study, the cell model of CT was used to replace the BB. Since the intercaval bundles are made up of atrial cells, the AP of atria (Courtemanche *et al*., 1998) was applied to them in our simulation.

2.4 Numerical analysis of excitation conduction model

The mono-domain equation is used to simulate the excitation conduction, which is expressed as follows (Whiteley, 2006):

$$\begin{aligned}&\frac{\partial V_{\mathrm{m}}}{\partial t}=\nabla(\boldsymbol{D}\cdot\nabla V_{\mathrm{m}})-(I_{\mathrm{ion}}+I_{\mathrm{applied}})/C_{\mathrm{m}},\\&\boldsymbol{D}=\boldsymbol{G}_{\mathrm{i}}/(S_{\mathrm{v}}\cdot C_{\mathrm{m}}),\end{aligned}\tag{1}$$

where S_{v} is the surface volume ratio of cells (μm^{-1}), with the value of 4 μm^{-1}. Since these cell models were based on the model of Courtemanche *et al*. (1998), all cell types in this study have the same S_{v} values. C_{m} is the specific capacitance (pF), $\boldsymbol{G}_{\mathrm{i}}$ is the bulk intracellular conductivity (mS/cm), V_{m} is the transmembrane potential (mV), I_{applied} is the transmembrane stimulating current density and I_{ion} is the sum of all transmembrane ionic currents (pA/pF). In this study, we used the finite difference method to calculate Eq. (1), because of its simplicity and suitability for the parallel computation.

2.5 Simulation protocol

In the following simulations, the anisotropic conduction situation was investigated first. Simulation via BB has been extensively investigated by many groups (Harrild and Henriquez, 2000; Seemann *et al*., 2006). Furthermore, the developed model in this study can be validated by comparing the corresponding simulation results. Conduction via CS, LFO, and the combination of BB, CS, and LFO were investigated next. In these conduction pathways (excluding BB), we also compared the two situations: with or without the two intercaval bundles connecting CT, LFO, and CS. The obtained simulation conduction patterns were explained in detail in each case. Finally, the isotropic conduction via BB was also investigated as an example of checking the difference between the anisotropic and isotropic conductions.

Experimental data showed that the anisotropy in the atria was not obvious (Hansson *et al*., 1998) and that the longitudinal and transversal ratio varied from 1.0 to 1.6 when cycle length was 160 ms (Gray *et al*., 1996). In order to study how the anisotropy affects the electrical conduction, the longitudinal and transverse ratio was set as 1.3, a midrange value between 1.0 and 1.6. With these settings, the conduction in the atria for both isotropic and anisotropic conductions was in accordance with the clinical data (Lemery *et al*., 2004; 2007; Jurkko, 2009). The details about these simulations were presented in the following sections.

3 Results

3.1 Normal electrical conduction via BB

The simulation results for the conduction pattern via BB without fast bundles are displayed in Fig. 3, and the associated parameter settings are listed in the first row of Table 1. From the excitation sequence as shown in Fig. 3, it can be seen that the earliest activation area in RA was located in the center of the SAN, followed by the periphery (after about 5 ms), then the wave spread arterially to the right atrial appendage (RAA) and upward to the roof of the superior vena cava (SVC). Meanwhile, the wave quickly spread downwards to the atrioventricular region along CT and leftwards to LA along BB (arrows 1 and 2 in Figs. 3a and 3b). The excitation also conducted to the PM (arrow 2 in Fig. 3c) and it can be seen that the conduction speed was slower from CT to PM than from CT itself and the wavefront was almost elliptic. At 30 ms, the wave spread to the junction of LA and RA in the posterior wall and to the upper part of RAA; most parts of the SVC were excited. At the same time, the excitation conducted to LA via BB (the solid circle in Fig. 3a), then the wave spread in all

directions. At 51 ms, the muscular rim of FO in RA was excited along with half of the RA. The activation descended the lateral wall, posterior wall, and septum in a uniform manner. At 81 ms, RA was excited completely. The last activation site was in the front of CS (the asterisk in Fig. 3c).

For LA, after it was activated via BB, the wave in the roof of LA conducted in all directions. At 81 ms, the anterior parts of LA and the left atrial appendage (LAA) were excited completely and there were three different wavefronts conducting towards the posterior wall: the first one came from the roof of LA (arrow 6 in Figs. 3a–3c); the second one from the LAA (arrow 5 in Figs. 3a–3c); and the third one from the septum of LA (arrow 7 in Figs. 3a–3c). After approximately 14 ms, the three wavefronts merged together and conducted to the area near mitral annular (arrows 5 and 7 in Figs. 3b and 3c). At 109 ms, the excitation wave ended in the middle of the bottom LA. The time of critical positions and the excitation time in atria were summarized in the first row of Table 2.

3.2 Normal electrical conduction via LFO

The simulation results for this condition with fast bundles are displayed in Figs. 4a–4c and the associated parameters are listed in the second row of

Table 1 Assigned conductivities in different conduction pathways

Conduction pathway	Conductivity (mS/cm)/average conduction speed (cm/s)									
	BB	CT	PM	LFO	FO	CS	LAM	RAM	IB1	IB2
Solitary BB without IB	107.2/113	125.1/115	125.1/123	0/0	0/0	0/0	19.7/76	25/85	0/0	0/0
Solitary LFO with IB	0/0	125.1/115	125.1/123	3.5/30	7.15/45	0/0	14.3/62	25/85	120/132	0/0
Solitary LFO without IB	0/0	125.1/115	125.1/123	3.5/30	7.15/45	0/0	25/85	25/85	0/0	0/0
Solitary CS with IB	0/0	125.1/115	125.1/123	0/0	0/0	10.7/50	26.8/87	25/85	0/0	120/132
Solitary CS without IB	0/0	125.1/115	125.1/123	0/0	0/0	10.7/50	19.7/76	25/85	0/0	0/0
BB+LFO with IB	107.2/113	125.1/115	125.1/123	3.5/30	7.15/45	0/0	10.72/54	25/85	120/132	0/0
BB+LFO without IB	107.2/113	125.1/115	125.1/123	3.5/30	7.15/45	0/0	14.3/62	25/85	0/0	0/0
BB+CS with IB	107.2/113	125.1/115	125.1/123	0/0	0/0	10.7/50	8.94/50	25/85	0/0	120/132
BB+CS without IB	107.2/113	125.1/115	125.1/123	0/0	0/0	10.7/50	12.51/58	25/85	0/0	0/0
LFO+CS with IB	0/0	125.1/115	125.1/123	3.5/30	7.15/45	10.7/50	14.3/62	25/85	120/132	120/132
LFO+CS without IB	0/0	125.1/115	125.1/123	3.5/30	7.15/45	10.7/50	25/85	25/85	0/0	0/0
BB+LFO+CS with IB	107.2/113	125.1/115	125.1/123	3.5/30	7.15/45	10.7/50	8.22/48	25/85	120/132	120/132
BB+LFO+CS without IB	107.2/113	125.1/115	125.1/123	3.5/30	7.15/45	10.7/50	14.3/62	25/85	0/0	0/0
Solitary BB without IB iso	53.61/110	35.74/115	35.74/123	0/0	0/0	0/0	19.7/76	25/85	0/0	0/0

BB: Bachmann's bundle; PM: pectinate muscles; FO: fossa ovalis; LFO: limbus of the fossa ovalis; CS: coronary sinus; CT: crista terminalis; RAM: right atrial muscles; LAM: left atrial muscles; IB1: intercaval bundle connets CT and LFO; IB2: intercaval bundle connets CT and CS; IB: the combination of IB1 and IB2; Iso: isotropic conduction

Table 2 Simulated earliest activation time and total activation time in different conduction pathways

Conduction pathway	Earliest activation time (ms)						Total activation time (ms)		
	BB left	BB right	FO left	FO right	CS left	CS right	LA	RA	Whole atria
Solitary BB with IB	30	18					79	81	109
Solitary LFO with IB			30	26			90	79	120
Solitary LFO without IB			55	51			71	81	126
Solitary CS with IB					41	34	68	81	109
Solitary CS without IB					82	75	80	81	162
BB+LFO with IB	30	18	30	26			89	79	119
BB+LFO without IB	30	18	55	51			87	81	117
BB+CS with IB	30	18			41	34	88	81	118
BB+CS without IB	30	18			82	75	88	81	118
LFO+CS with IB			30	26	41	34	85	81	115
LFO+CS without IB			55	51	82	75	71	81	126
BB+LFO+CS with IB	30	18	30	26	41	34	86	79	116
BB+LFO+CS without IB	30	18	55	51	82	75	87	81	117
Solitary BB without IB iso	32	17					77	82	109

BB: Bachmann's bundle; FO: fossa ovalis; LFO: limbus of the fossa ovalis; CS: coronary sinus; IB1: intercaval bundle connets CT and LFO; IB2: intercaval bundle connets CT and CS. IB: the combination of IB1 and IB2; Iso: isotropic conduction; LA: left atrium; RA: right atrium

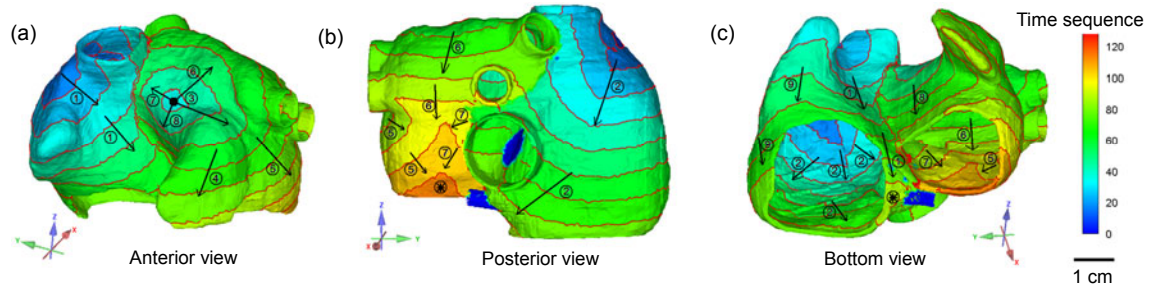

Fig. 3 Conduction pattern via BB without fast bundles

(a–c) are the excitation conduction sequences. The red lines are the isochrones, the black solid circle is the left insertion of BB and is the earliest activation position in LA. The arrows represent the wave spread directions, and they are distinguished by different numbers. The black asterisk in (b) is the last activation site of LA, the black asterisk in (c) is the last activation site of RA. The following figures used the same representations (Note: for interpretation of the references to color in this figure legend, the reader is referred to the web version of this article)

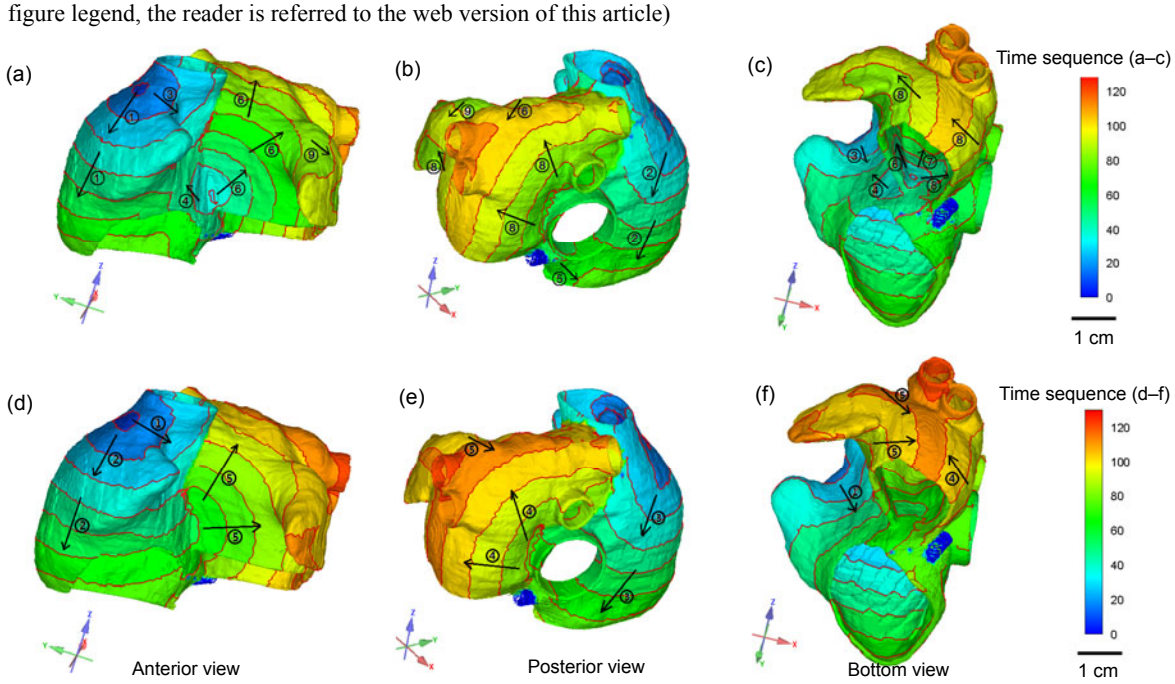

Fig. 4 Conduction pattern via LFO

(a–c) are the excitation conduction sequences via LFO with fast bundles, (d–f) without fast bundles

Table 1. It can be seen that before the wave conducted to FO, the conduction pattern in RA was similar to the BB case, but after that, the conduction patterns in the right atrial septum changed a lot.

At 30 ms, the muscular rim of FO in RA was excited, then the wavefront conducted upwards to meet the wavefront from SVC, forwards to activate the anterior part of RA (arrow 4 in Figs. 4a and 4c), and downwards to the isthmus (arrow 5 in Fig. 4b). At 43 ms, the FO was almost excited and the wavefronts from LFO and SVC began to merge. Later, the CS began to excite and the wavefront spread to the isthmus. At 78 ms the entire RA was excited and the last activation site was the vicinity of atrioventricular ring (AVR). For RA, the anterior wall was activated by the wavefronts from SAN and FO, but the lateral wall and most of the posterior wall were activated by the wavefront from SAN.

When the wavefront conducted to LA via LFO, it began to spread in all directions (arrows 6, 7, and 8 in Fig. 4c): anterior wall, posterior wall, and the upper part of septum, then the wavefronts began to activate the anterior and posterior walls. At 90 ms, half of the LAA lateral wall and the left atrial posterior wall had been excited. The excitation sequence showed that the LAA was activated by the wavefront from the anterior

wall and that the roof of LA and lateral wall were activated by the wavefronts from the anterior wall and posterior wall (arrows 8 and 9 in Fig. 4b). At 120 ms, the last activation site-left superior pulmonary vein (LSPV) was excited. The time of critical positions and the excitation time in atria were summarized in the second row of Table 2.

Figs. 4d–4f show the simulation results without the fast bundles. Compared with the FO conduction with fast conduction bundle, the right atrial conduction pattern was similar to the conduction via BB in that they both conducted the excitation from SAN downwards to the atrioventricular node (AVN) (Figs. 4d and 4e), but when the fast conduction bundle was included in the FO conduction, the wavefront from the FO spread upward to collide with the wavefront that originated from SAN, and downward to the cavotricuspid isthmus to meet the wavefront from CT, the last activation site located at the bottom of posterior and lateral walls of RA. Although the total atrial activation time (120 ms vs. 126 ms) and activation pattern in LA were similar between the two conduction types, the left atrial activation time and the conductivites differed greatly.

Without fast bundle, the whole left atrial activation time was 71 ms, which was far slower than the conduction with fast bundle (90 ms). The activation time is shown in the third row in Table 2.

3.3 Normal electrical conduction via CS

For this condition, the simulation results with fast bundles are displayed in Figs. 5a–5c, and the associated parameter settings are listed in the fourth row of Table 1. At 41 ms, the excitation conducted from SAN to LA where the distal CS and LA joined via the CS, and then the wavefront spread to the roof of LA radically (arrows 4, 5, and 6 in Figs. 5a–5c). The RA activation pattern was similar to that of the BB case.

At 55 ms, the wavefront conducted to the floor of FO and then it spread to the anterior wall of LA and upward to the roof of LA (arrows 5 and 6 in Figs. 5a and 5b). At 90 ms, the wavefronts from the anterior and lateral walls met at the floor of LAA then they conducted upward to the lateral wall of LAA and to the roof of LA (arrows 4, 7, and 8 in Figs. 5a and 5c).

At 104 ms, the wavefronts from the roof and floor of LAA began to merge at the lateral wall and the wavefronts from the anterior and posterior walls of LA began to merge at the roof of LA. The last activated area was the tip of LAA and right superior pulmonary vein (RSPV) which occurred at 109 ms. The activation time is shown in the fourth row of Table 2.

The simulation results without the intercaval bundle (IB2 in Table 1) are displayed in Figs. 5d–5f,

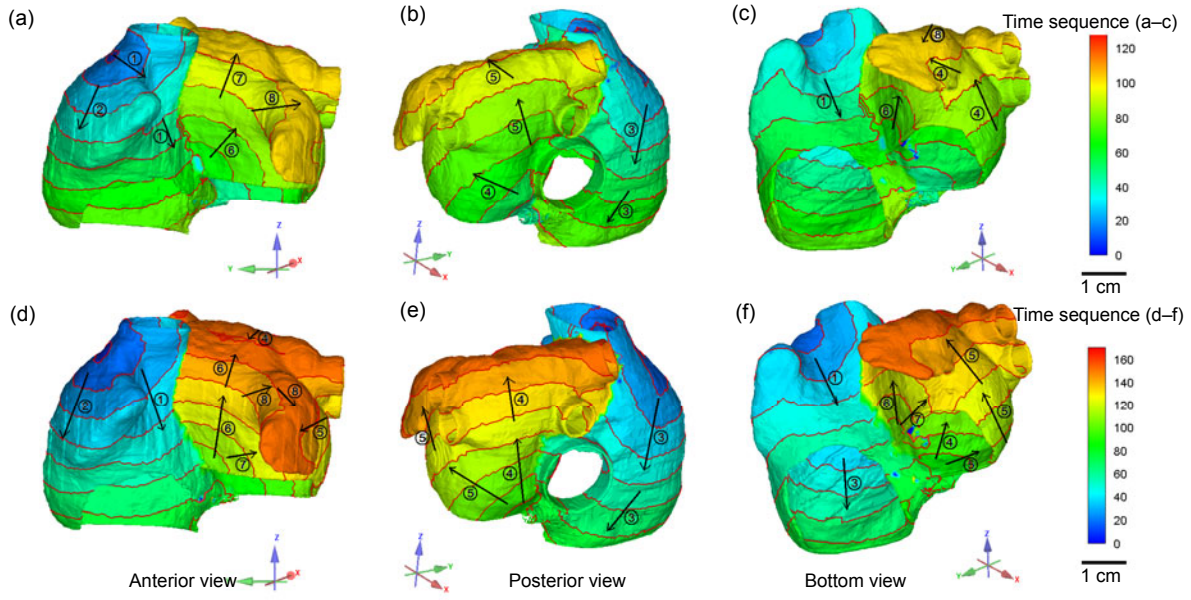

Fig. 5 Conduction pattern via CS

(a–c) are the excitation conduction sequences via CS with fast bundles, (d–f) without fast bundles

and the associated conductivities are listed in the fifth row of Table 1. Compared with the CS conduction with fast bundle, the RA conduction pattern was slightly different, while the LA conduction pattern was significantly different (Figs. 5d–5f). In our simulation, the conduction time via CS without fast bundle was 162 ms, which was much longer than that shown by Jurkko *et al*. (2009; 2010). The associated conduction speed was approximately 70 cm/s, and the left atrial conduction time was 80 ms (the earliest activation time of LA was 82 ms), which was close to the left atrial conduction time (~80 ms) shown by other studies (Roithinger *et al*., 1999; de Ponti *et al*., 2002; Lemery *et al*., 2007). If the conductivity of LA was increased to 28.6 mS/cm, the associated conduction speed was approximately 90 cm/s, but the activation time of whole atria was still more than 140 ms. The activation time is shown in the fifth row of Table 2.

3.4 Normal electrical conduction via BB and LFO

The conductivity pattern for the simulation with the intercaval bundle that connects the origins of CT and LFO is listed in the sixth row of Table 1 and the results are displayed in Figs. 6a–6c. In this case, before the merger of the two wavefronts from BB and LFO, the conduction pattern in LA was the combination of BB and LFO.

At 57 ms, the wavefront from BB began to merge with the wavefront from LFO at the anterior middle wall (arrows 8 and 11 in Fig. 6a), and then the wavefront conducted to the lateral wall of LA and medial wall of LAA (arrow 11 in Fig. 6a). At 92 ms, the wavefront from the left atrial posterior wall began to merge with the wavefront from the roof of LA (arrows 6 and 10 in Fig. 6b). Meanwhile, the wavefront from the roof of LA merged with the wavefront from the anterior wall at the conjunction of LAA and LA (arrows 11 and 12 in Fig. 6c).

At 106 ms, the wavefronts from the posterior wall and the roof of LA ended at the vicinity of the left inferior pulmonary vein (LIPV), and the wavefronts from the posterior and lateral walls merged and ended at the lateral wall close to the AVR at 119 ms (arrows 10, 11, and 12 in Figs. 6b and 6c). The activation time is shown in the sixth row of Table 2.

The results of the simulation when the intercaval bundle (IB1 in Table 1) was not introduced are displayed in Figs. 6d–6f, and the associated conductivities are listed in the seventh row of Table 1. Since both the BB and LFO can conduct the excitation, the wave spread in the LA was the combination of the conductions via BB and FO.

Compared with the conduction with intercaval bundle, the merging time of wavefronts from BB and

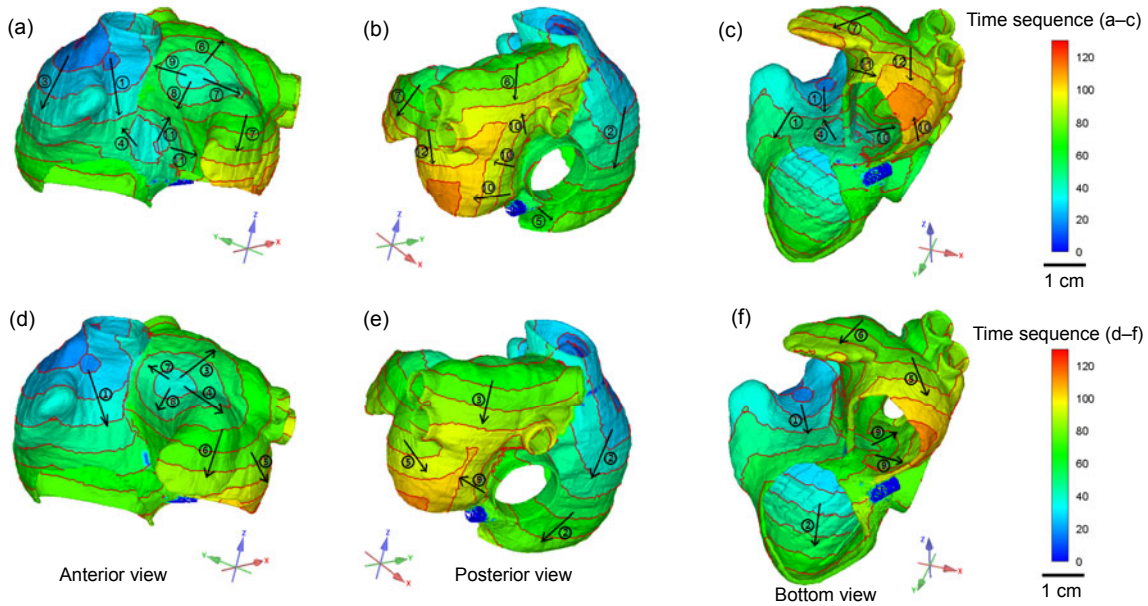

Fig. 6 Conduction pattern via BB and LFO

(a–c) are excitation conduction sequences via BB and LFO with fast bundles, (d–f) without fast bundles

FO was longer (57 ms vs. 65 ms) and the merging site (close to the left atrial septum) was lower. When intercaval bundle was introduced, the anterior wall was activated by both the wavefronts from BB and FO and most of the posterior wall was activated by the wavefront from BB, but if the intercaval bundle was not introduced, the most of anterior wall was activated by the wavefront from BB, and the posterior wall was activated by both wavefronts from BB and FO.

At 94 ms, the wavefronts from the left atrial septum and lateral wall had merged with the wavefront from the upper part of LA. After 6 ms, the three wavefronts merged together at the middle part of the posterior wall of LA (arrows 3, 5, and 9 in Figs. 6e and 6f). At 117 ms, the wavefront conducted to the posterolateral wall under the left pulmonary vein and ended it the atrial depolarization. The activation time is shown in the seventh row of Table 2.

3.5 Normal electrical conduction via BB and CS

The conductivity pattern with the intercaval bundle that connects the origins of CT and CS is listed in the eighth row of Table 1 and the results are displayed in Figs. 7a–7c. In this case, before the merging of the two wavefronts from BB and CS, the conduction pattern in LA was a combination of BB and CS.

At 86 ms, the wavefront from BB began to merge with the wavefront from CS at the anterior wall close to the septum (arrows 7 and 11 in Fig. 7c), and then the wavefront conducted to the lateral wall of LA. At 92 ms, the wavefront from BB merged with the wavefront from the lateral wall of LAA at the conjunction of LAA and LA (arrows 7 and 8 in Fig. 7c) and then it conducted upward to meet the wavefront from the roof of LA at the middle part of the posterior wall at 109 ms (arrows 5 and 11 in Fig. 7b). Meanwhile, the wavefront from the lower part of the posterior wall merged with the wavefront from LAA at the lower part of the lateral wall of LA (arrows 8 and 12 in Figs. 7a–7c). The last activation site was the right inferior pulmonary vein at 118 ms. The activation time is shown in the eighth row of Table 2.

The simulation results without the intercaval bundle (IB2 in Table 1) are displayed in Figs. 7d–7f, and the associated conductivities are listed in the ninth of Table 1. Compared with the conduction with intercaval bundle, the merging time of wavefronts from BB and CS was much longer (86 ms vs. 97 ms) and the merging site was much lower (at the floor of FO). When intercaval bundle was introduced, the lateral and posterior walls were activated by both wavefronts from BB and CS, but if not introduced, the lateral wall was activated by the wavefront from BB and only about one third of the posterior wall was activated by the wavefront from CS. The last activation sites were different too; one located at the posterior wall close to the atrioventricular ring and the other located at the lateral and the posterior walls close to LIPV. The activation time is shown in the ninth row of Table 2.

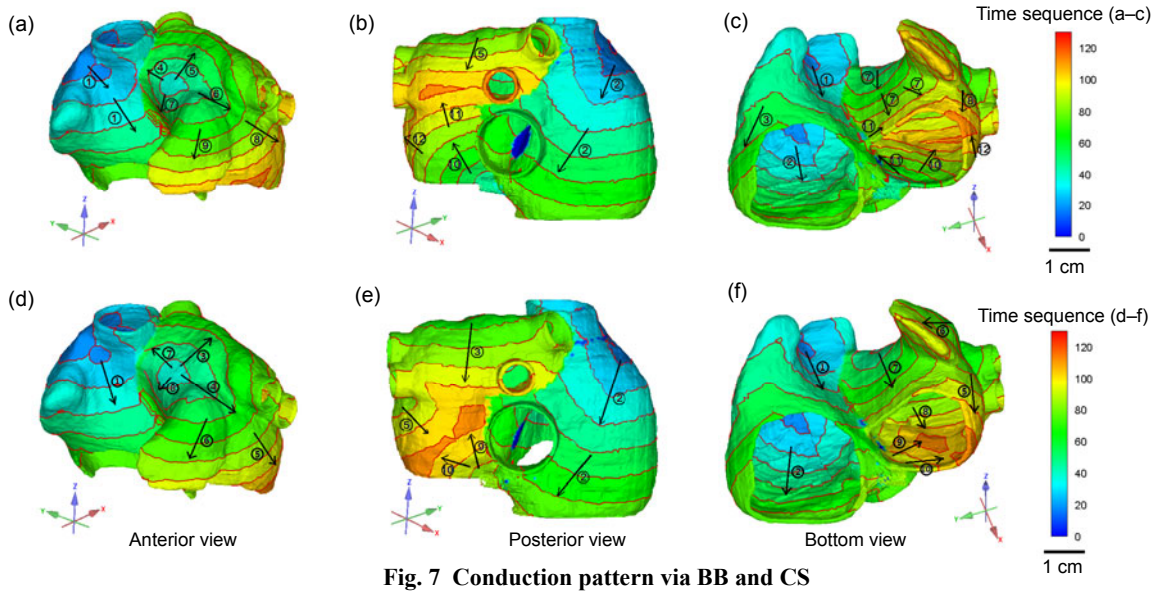

Fig. 7 Conduction pattern via BB and CS

(a–c) are excitation conduction sequences via BB and CS with fast bundles, (d–f) without fast bundles

3.6 Normal electrical conduction via LFO and CS

Pattern conductivities when the two intercaval bundles that connect the origins of CT, CS and LFO were introduced are listed in the 10th row of Table 1 and the results are displayed in Fig. 8. In this case, before the two wavefronts from LFO and CS merged, the conduction pattern in LA was a combination of LFO and CS.

At 54 ms, the wavefronts from the LFO and CS began to merge at the floor of FO then the wavefront conducted upward to the roof of LA and leftwards to the posterior wall (arrows 11 and 12 in Fig. 8c). At 91 ms, the two wavefronts from the posterior and anterior walls began to merge. Meanwhile, the wavefronts from the roof and floor of LAA had merged at the lateral wall of LAA (arrows 8 to 11 in Figs. 8a–8c).

At 102 ms, the lateral wall of LA had been activated and meanwhile, the two wavefronts from the root of atria and posterior wall had already merged and conducted towards the left pulmonary vein (arrows 6 and 12 in Figs. 8a and 8b). After 14 ms, the entire atria had been activated and the last activation site was the LSPV. The activation time is shown in the 10th row of Table 2.

Pattern conductivities when the two intercaval bundles (IB in Table 1) were not introduced are listed in the 11th row of Table 1. The conduction pattern via FO and CS was same as that via unique FO since the wavefront via CS conducted to the junction of distal CS and LA at the same time as the wavefront via FO. The activation time is shown in the 11th row of Table 2.

3.7 Normal electrical conduction via BB, LFO, and CS

Pattern conductivities when the two intercaval bundles which connect the origin of CT, CS, and LFO were introduced are listed in the 12th row of Table 1 and the results are displayed in Fig. 9. In this case, before the three wavefronts from BB, LFO, and CS merged, the conduction pattern in LA was a combination of BB, LFO, and CS.

At 56 ms, the two wavefronts from BB and LFO began to merge at the anterior wall then the wavefront conducted leftward to the lateral wall of LA and LAA (arrows 7 to 11 in Figs. 9a and 9c). Meanwhile, the wavefront from LFO began to merge with the wavefront from CS at the floor of FO and then conducted to the posterior wall (arrows 12 and 16 in Fig. 9c).

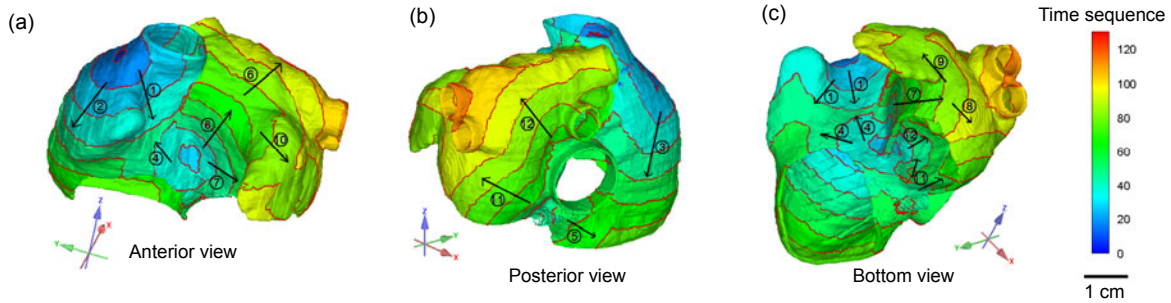

Fig. 8 Conduction pattern via LFO and CS

(a–c) are the excitation conduction sequences via LFO and CS with fast bundles

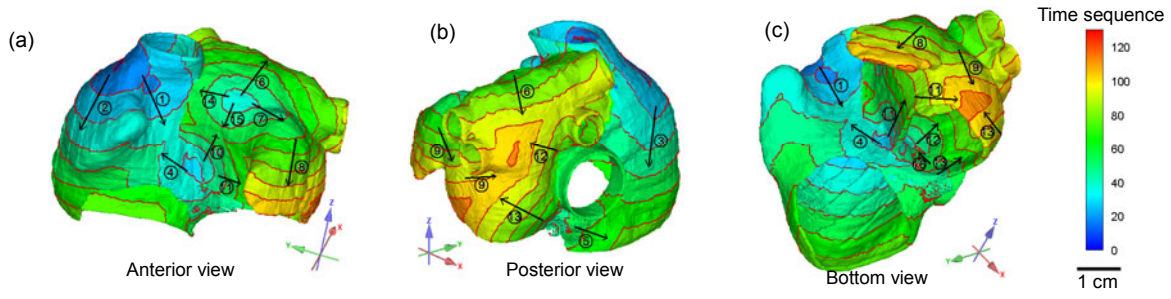

Fig. 9 Conduction pattern via BB, LFO, and CS

(a–c) are the excitation conduction sequences via BB, LFO, and CS with fast bundles

At 95 ms, the wavefront from the roof of LA began to merge with the wavefront from the posterior wall (arrows 6 and 12 in Fig. 9b) and meanwhile, the wavefront from the roof of LA had merged with the wavefront from the anterior wall at the conjunction of LAA and LA (arrows 9 and 11 in Fig. 9c). At 107 ms, the three wavefronts from the roof of atria, the posterior wall, and the lateral wall had merged together, and ended at the vicinity of LIPV at 112 ms (arrows 9, 12, and 13 in Fig. 9b). The last activation site was the lateral wall close to the AVR and the activation time of the whole heart was 116 ms (arrows 9, 11, and 13 in Fig. 9c). The activation time is shown in the 12th row of Table 2.

The conductivity pattern when the two intercaval bundles (IB in Table 1) were not included is listed in the 13th row of Table 1 and the activation time is shown in the 13th row of Table 2. The conduction pattern via BB, FO, and CS was the same as that via BB and FO.

3.8 Isotropic conduction via BB

For the isotropic conduction, we only simulated the conduction via BB, since there is no major difference between the conductions via BB and other pathways. The associated conductivities are listed in the 14th row of Table 1, and the results are shown in Fig. 10. The activation time is shown in the 14th row of Table 2.

For the conduction pattern, the isotropic and anisotropic conductions had only small differences such as the left atrial activation time and the total conduction time of LA and RA. The activation time of FO in isotropic conduction was 55 ms, which is longer than that of the anisotropic conduction (51 ms). The biggest difference is that the conductivities of the conduction system in atria were much smaller for the isotropic conduction than for the anisotropic conduction.

4 Discussion

In this study, we presented simulation of the biatrial conduction via various pathways using a detailed anatomic atrial model with realistically measured myofiber orientation data. The pathways investigated in this study include BB, CS, LFO, and the two intercaval bundles, which connect CT, LFO, and CS. For the first time, the two assumed intercaval bundles were studied in detail and the anisotropic conductions with these pathways were compared. The atrial conduction time and the activation sequences in our simulation were generally in agreement with clinical data (Boineau *et al*., 1988; de Ponti *et al*., 2002; Lemery *et al*., 2004; 2007; Jurkko *et al*., 2009; 2010; Tapanainen *et al*., 2009). Tables 3 and 4 list the experimental data from different studies.

In our study, the spatial resolution of atrial anatomic model is approximately 0.35 mm, which is finer than other models. For example, the spatial resolution of the model developed by Lorange and Gulrajani (1993) is 1 mm and that of Lu *et al*. (1993) is 1.5 mm. A detailed human atrial anatomy model was constructed by Harrild and Henriquez (2000) with a mean interelement distance is 0.55 mm; however, the drawback of that model is that it was constructed from reports, not real human atria. In a human atrial monolayer model constructed using MRI (Blanc *et al*., 2001), the mean edge length of the epicardial meshes in high quality is 0.434 mm. The spatial resolution of the Visible Female datasets is 0.33 mm (Sachse *et al*., 2000) which is finer than that of our model, but is limited in that it cannot provide the fiber information that

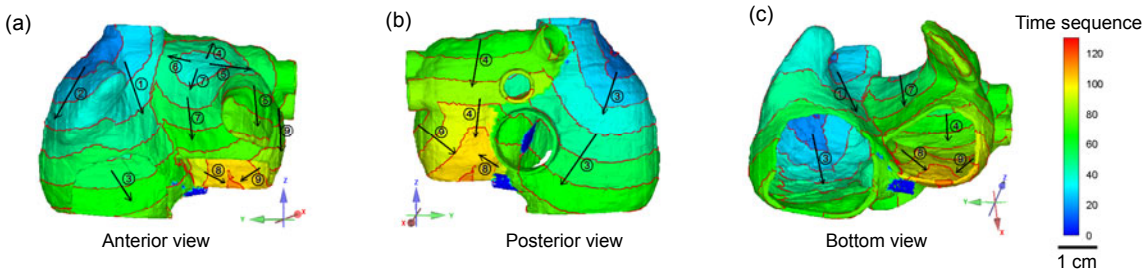

Fig. 10 Isotropic conduction via BB without fast bundles
(a–c) are the excitation conduction sequences

Table 3 Experimental data of earliest activation time and total activation time in different conduction pathways

Reference		Earliest activation time (ms)						Total activation time (ms)		
		BB left	BB right	FO left	FO right	CS left	CS right	LA	RA	Whole atria
Lemery *et al*., 2004		41±18	19±12	43±17	24±9			80±11	81±18	120±24
de Ponti *et al*., 2002		30±6		39±5	42±5			81±10	92±10	105±9
Markides *et al*., 2003		26±2						65±4		134±3
Lemery *et al*., 2007		31±13		52±15	45±14	95±34	84±17		93±17	116±18
Jurkko, 2009										
Study III	BB	41±14						81±16		121±15
	CS					34±9		80±9		114±13
	FO			29±11				93±7		124±11
	Combined				35±10*			84±12		118±11
Study IV	BB	34±8						81±10		116±10
	CS					40±11		62±14		102±3
	FO			32±4				91±11		123±11
	Combined				32±10*			88±14		120±13

BB: Bachmann's bundle; FO: fossa ovalis; CS: coronary sinus; LA: left atrium; RA: right atrium. * Value is combined earliest activation time

Table 4 Experimental data of conduction speed of different parts in atria

Tissue name	Conduction speed (cm/s)	Reference
BB	92–167	Dolber and Spach, 1989
CT	70–130	Boineau *et al*., 1980; Boineau, 1985
PM	117–154	Hayashi *et al*., 1982
LAM	68–103	Hansson *et al*., 1998
	70.2±9.9	Kojodjojo *et al*., 2006
RAM	68–103	Hansson *et al*., 1998
	77.0±10.8	Kojodjojo *et al*., 2006

BB: Bachmann's bundle; PM: pectinate muscles; CT: crista terminalis; RAM: right atrial muscles; LAM: left atrial muscles

is important in anisotropic simulation.

Although the fiber orientation in our model is monolayer and its spatial resolution is not high, it does present improvements in atrial simulation. Until recently, a set of quantitatively measured data of whole atria has been lacking, limiting the ability to conduct realistic anisotropic conduction simulation in normal conditions. In addition, our model provides realistic fiber orientation, which improves on past models.

4.1 Assignment of conductivities

In our simulation, our conductivities were consistently larger than that published by Harrild and Henriquez (2000) for two reasons. First, the anisotropy ratio in our model was larger (9.00 vs. 7.54 for CT and PM, 1.3 vs. 1.0 for atrial muscles). Since the spatial resolution can affect the conductivities, it is expected that higher spatial resolution will quicken the conduction speed (ten Tusscher *et al*., 2004). In our model, the spatial resolution was 0.3574 mm, so larger conductivities should be assigned.

Second, for the source sink effect, in the Harrild and Henriquez (2000)'s model, PM only connects to atrial muscles at their midpoints and ends but in our model the PM and atrial muscles connect with each other and the PM must excite much more atrial cells. Because this connection slows the conduction speed, larger conductivities were assigned to compensate. It is known that for LA the conduction time through different pathways varies greatly (Jurkko, 2009), so in order to attain realistic conduction time and speed, the conductivities were also varied.

For the SAN modeling, from the original paper (Chandler *et al*., 2009) we can see that the paranodal area (peripheral cells in our simulation) demonstrated an intermediate pattern of expression of many ion channels similar to that seen in the periphery of the rabbit sinus node (Tellez *et al*., 2006). The paranodal area, however, shows a unique pattern of expression of K^+ channels and accessory subunits. So the peripheral cell in Chandler *et al*. (2009) is different from the periphery cell in Zhang *et al*. (2000). To our knowledge, since the paper from Chandler *et al*. (2009) is the only one that systematically studies the human SAN, more experimental data are required to validate their findings. Finally, in normal conduction, the autorhythmicity of peripheral cells in SAN is suppressed by

the center cell of SAN, so autorhythmicity will have no impact on the normal biatrial conduction.

4.2 Right atrial conduction

In normal state, the conduction via BB was the most dominant pathway (Lemery *et al*., 2004; Jurkko *et al*., 2010); because we set the conductivities in CS and LFO to 0, the BB was the only conduction pathway between RA and LA. In our simulation the SAN was located in the groove between the RAA and the lateral atrial wall (Anderson *et al*., 1979; James, 2002) and contained the central and peripheral parts. The center part showed a higher frequency of autorhythmicity which dominated the heart rate and only conducted the electrical activation to periphery cells. Recently, Fedorov *et al*. (2010) showed that the SAN was functionally insulated from the surrounding atrial myocytes except for a limited number of exit sites. Therefore, in our simulation the excitation from the periphery cells can only conduct to the CT. With these settings the time of excitation from SAN to the epicardial was 7 ms and was similar to the measured clinical data ((11±18) ms) (Lemery *et al*., 2007).

When CT and PM were excited, the wave spread to the surrounding atrial cells. The conduction velocity in the right atrial wall was not homogenous: the velocity of the posterolateral wall with PM was 70 to 100 cm/s and the average velocity was close to 95 cm/s. These results can be explained by the fact that, in our model, the PM and atrial muscles connected with each other and the PM displayed higher conduction velocity. This phenomenon has also been reported in experimental data (Wu *et al*., 1998) and another atrial model although the PM and atrial wall was set to contact at certain points (Harrild and Henriquez, 2000). The conduction speed of the smooth septum wall and anterior wall was far slower than that of the posterolateral wall with PMs, ranging from 70 to 90 cm/s with an average value of 85 cm/s, which falls in the range of previously reported results of −68 to 103 cm/s (Hansson *et al*., 1998).

4.3 Left atrial conduction via BB

When the atrial electrical conduction was through BB, the earliest excited site was located in the anterior left atrial wall, but the earliest activation time varied. de Ponti *et al*. (2002) reported that the value of earliest activation time of LA was (30±6) ms, while the earliest activation time was (26±2) ms in Markides *et al*. (2003). It has previously been reported that the RA insertion of BB was activated at (41±18) ms (Lemery *et al*., 2004) and that conduction over BB resulted in earliest left atrial activation endocardially at (31±13) ms (Lemery *et al*., 2007). Recently, Tapanainen *et al*. (2009) reported that if FO was involved in the atrial conduction, the earliest activation time was (31±9) ms, otherwise, the time was (39±14) ms. Another study reported that left atrial activation started at 34 ms on average (Jurkko *et al*., 2009). In our simulation, the earliest activation time in LA was 30 ms, similar to another computer simulation report of 29.7 ms (Harrild and Henriquez, 2000).

There is little experimental data about the total conduction time for the BB, partly because the SAN and BB are too close and therefore it is hard to measure the early activation time in the right insertion of BB. Nevertheless, Lemery *et al*. (2004) reported that the quantitatively measured total BB conduction time was (23±15) ms. Our simulated result was 16 ms, which was a little shorter than the average value but within the reported range. The conduction velocity of BB in our simulation was between 95 to 150 cm/s and the average velocity was 113 cm/s, falling within the range reported by Dolber and Spach (1989).

In our simulation, the total activation times of LA and whole atria were 79 and 109 ms, respectively. de Ponti *et al*. (2002) reported that the durations of left atrial propagation and whole atria were (81±10) and (105±9) ms, respectively. Our study results are similar to previous reports that determined the activation times of LA and whole atria to be (80±11) and (120±24) ms, respectively (Lemery *et al*., 2004), and (84±14) and (119±14) ms, respectively (Tapanainen *et al*., 2009).

4.4 Left atrial conduction via LFO and CS

The experimental data showed that the first activation time in LA via solitary CS conduction was (34±9) ms in Study III and (40±11) ms in Study IV (Jurkko, 2009). We believe that the reason why the activation time was much earlier than that of the other experimental data (de Ponti *et al*., 2002; Lemery *et al*., 2004; 2007) is that the results of the latter groups were for the atrial conduction via solitary BB or combination of BB, CS, and LFO.

When the atrial conduction is via solitary CS or LFO, the earliest activation time in LA was very short (Jurkko, 2009). In our simulation we assumed that there existed muscle bundles between the origins of CT and CS and LFO and that this would conduct excitation from SAN to CS and LFO faster than the surrounding atrial muscles. The existence of these pathways is supported by anatomical evidence.

Ho *et al*. (2002a) described that the peripheral fibers around the fossa in the antero-superior rim extend toward the origin of the terminal crest. Wang *et al*. (1995) showed that some muscle bundles passed from the SAN to the vicinity of the FO; the authors claimed that the excitation wave may spread from the SAN to the interatrial septum along the anterior rim of the oval fossa. In addition they also showed some muscle bundles connected the origin of CT and the vicinity of CS.

Tapanainen *et al*. (2009) suggested that the earlier activation time in LA via LFO instead of BB was possible due to the extent and location of the connecting fibers and differences in conduction velocities within the atria. In addition, computer simulations have included the intercaval bundle between CT and LFO (Harrild and Henriquez, 2000).

Sun and Khoury (2001) studied the electrical conduction within the inferior atrial region and showed that sinus rhythm activation initiated in superior RA at the junction of the posterior and lateral walls propagated in anterior directions and bypassed the anterior rim of the FO toward the CS.

In our simulation, the geometry of the two pathways was based on general descriptions (Wang *et al*., 1995; Sun and Khoury, 2001; Ho *et al*., 2002a). While detailed description of the muscle structures in the vicinities of the interatrial septum and CS was lacking, these reports contained some qualitative description and images to support their viewpoint. Nevertheless, most of anatomists agree with these points and the debate is about whether these quicker conduction muscles are made up of working atrial myocardial fibers or special myocardial cells. In our simulation we choose the geometry of the assumed pathways based on these guide lines. To our knowledge, this is the first model containing the two pathways in biatrial conduction simulation. The model by Harrild and Henriquez (2000) only contained one pathway connecting the midpoint of CT and FO.

Due to the lack of accurate experimental data, an accurate geometry of the two pathways cannot be obtained from our simulation, but if these two pathways had been excluded the results would have been significantly different from the experiential data (Jurkko, 2009). We suggest that although the geometry of the two pathways may vary they should not be excluded from the model.

4.5 Factors for differing activation time of LA

In our model, we assumed that there existed muscle bundles between the origins of CT and CS and FO and that they were composed of normal atrial muscles but that they had a high anisotropy ratio. Although our hypothesis can explain the differences between the activation time of LA and the whole atrial activation time, we cannot exclude other factors that may influence the earliest activation time of LA.

First, the sinus node is normally located in a relatively limited area in the high posterolateral RA but its location can vary within a 7.5 cm×1.5 cm area along RA and caval vein junction (Boineau *et al*., 1988; Cosio *et al*., 2004; Lemery *et al*., 2007). If SAN locates in the lower part, the conduction time from SAN to FO or CS may be shortened. Second, both the site of pace marker and the site out of the node can vary (Bromberg *et al*., 1995; Fedorov *et al*., 2010). Third, in the sinus node region the shift of impulse initiation alters with increasing rate upwards and with decreasing rate downwards (Boineau *et al*., 1988; Fedorov *et al*., 2010). In consideration of all these factors, our opinion is that the most important factor may be the existence of some bundles in the RA that can conduct the excitation faster than the working atrial myofibers.

4.6 Slow conduction via LFO

Our simulation results and the experimental data of Jurkko (2009) and Tapanainen *et al*. (2009) showed that if the LFO with the fast bundles was part of the conduction pathway, the duration of left atrial activation lasted longer (about 90 ms in LFO conduction vs. about 80 ms in other cases in our simulation). This may be due to the functional conduction block in LA. Markides *et al*. (2003) reported that there existed a functional conduction block in LA,

which originated in the anterior interatrial groove on the anterior left atrial wall and ended at the septal mitral annulus.

When LFO is the conduction pathway, the wavefront from LFO cannot conduct to the posterior wall but can only conduct to the roof of LA and then pass through the functional conduction line to activate the remaining part of LA. For BB, the left insertion is located at the anterior wall of LA (Lemery *et al*., 2003; Khaja and Flaker, 2005) and the functional conduction line was behind the anterior interatrial band (BB) (Markides *et al*., 2003); therefore, it cannot block the excitation from BB. For CS, the left insertion is located behind the functional conduction line and the line close to the septal mitral annulus was less distinct or even absent so the wavefront from CS can spread to the anterior wall and posterior wall in most cases.

4.7 Differences between isotropic and anistropic conditions

In our simulation the conductivities for BB, CT and PM in the anisotropic conduction were much greater than those in the isotropic conduction but there was almost no difference in the speed of conduction. The reason for this may be that during isotropic conduction the cells had stronger coupling and small conductivities can produce higher conduction speed. The conduction pattern was almost the same between isotropic and anisotropic conductions since the anisotropic ratio for atrial working myocardium was small.

Gray *et al*. (1996) reported that the anisotropic ratio for sheep epicardial wall was different from 1 and was 1.6 at the cycle length of stimulation (BCL)=160 ms. In our simulation, the anisotropic ratio was set to 1.3. From our simulation we can see that in the normal conduction the atrial working myocardium can be assumed to be isotropic conduction and it was used by many groups to simulate the atrial normal conduction (Harrild and Henriquez, 2000; Seemann *et al*., 2006). Koura *et al*. (2002) reported that the anisotropic ratio of the conduction velocity increased with increasing age and that the highest ratio was more than 1.5. When the atria have structural remodeling, the fibrosis will increase (Kamkin *et al*., 2003; Everett *et al*., 2006; Tanaka *et al*., 2007), which leads to the increase in anisotropic ratio in the atria and can make the AF easier to maintain and sustain. Therefore, the fiber orientation did not play a significant role in the normal atrial conduction but it may greatly influence wave conduction in pathologic conditions (Jacquemet *et al*., 2003; Deng and Xia, 2010).

4.8 Limitations

Although our anatomic model contained the detailed fast conduction bundles which are important for atrial conduction, they were not constructed based on scanned computerized tomography images due to limited spatial resolution. This may have resulted in data that are inconsistent with clinical data. The fiber orientation in our simulation only contained the epicardial wall, while the anatomic dissection showed that the myoarchitecture changes from subepicardium to subendocardium in LA. Furthermore, the fiber orientation in the anterior and septum wall in our model was based on other references so the simulated results may not be very precise.

Another limitation may be that the AP model of atrial cells was based on the Courtemanche *et al*. (1998) (CRN model) rather than a newer human atrial cell model published by Maleckar *et al*. (2009) (Maleckar model) which was based on the Nygren *et al*. (1998) model (NYG model). The main difference between the Maleckar and NYG models was revision of the repolarization current while leaving the depolarization relatively unchanged. Although the CRN and NYG models were derived from similar human atrial current data, their properties varied a lot (Cherry and Evans, 2008; Cherry *et al*., 2008), so the atrial conduction pattern achieved with the CRN model may be different from that of the Maleckar model. Future studies will investigate difference between these two models.

References

Anderson, K.R., Ho, S.Y., Anderson, R.H., 1979. Location and vascular supply of sinus node in human heart. *Br. Heart J*., **41**(1):28-32. [doi:10.1136/hrt.41.1.28]

Anderson, R.H., Cook, A.C., 2007. The structure and components of the atrial chambers. *Europace*, **9**(S6):vi3-vi9. [doi:10.1093/europace/eum200]

Anderson, R.H., Ho, S.Y., Becker, A.E., 2000. Anatomy of the human atrioventricular junctions revisited. *Anat. Rec*., **260**(1):81-91. [doi:10.1002/1097-0185(20000901)260:1<81::AID-AR90>3.0.CO;2-3]

Anderson, R.H., Yanni, J., Boyett, M.R., Chandler, N.J., Dobrzynski, H., 2009. The anatomy of the cardiac

conduction system. *Clin. Anat.*, **22**(1):99-113. [doi:10.1002/ca.20700]

Blanc, O., Virag, N., Vesin, J.M., Kappenberger, L., 2001. A computer model of human atria with reasonable computation load and realistic anatomical properties. *IEEE Trans. Biomed. Eng.*, **48**(11):1229-1237. [doi:10.1109/10.959315]

Boineau, J.P., 1985. Atrial flutter: a synthesis of concepts. *Circulation*, **72**(2):249-257. [doi:10.1161/01.CIR.72.2.249]

Boineau, J.P., Schuessler, R.B., Hackel, D.B., Miller, C.B., Brockus, C.W., Wylds, A.C., 1980. Widespread distribution and rate differentiation of the atrial pacemaker complex. *Am. J. Physiol.*, **239**(3):H406-H415.

Boineau, J.P., Canavan, T.E., Schuessler, R.B., Cain, M.E., Corr, P.B., Cox, J.L., 1988. Demonstration of a widely distributed atrial pacemaker complex in the human-heart. *Circulation*, **77**(6):1221-1237. [doi:10.1161/01.CIR.77.6.1221]

Bromberg, B.I., Hand, D.E., Schuessler, R.B., Boineau, J.P., 1995. Primary negativity does not predict dominant pacemaker location: implications for sinoatrial conduction. *Am. J. Physiol.*, **269**(3):H877-H887.

Burashnikov, A., Mannava, S., Antzelevitch, C., 2004. Transmembrane action potential heterogeneity in the canine isolated arterially perfused right atrium: effect of I_{kr} and I_{kur}/I_{to} block. *Am. J. Physiol.*, **286**(6):H2393-H2400. [doi:10.1152/ajpheart.01242.2003]

Chandler, N.J., Greener, I.D., Tellez, J.O., Inada, S., Musa, H., Molenaar, P., Difrancesco, D., Baruscotti, M., Longhi, R., Anderson, R.H., *et al.*, 2009. Molecular architecture of the human sinus node insights into the function of the cardiac pacemaker. *Circulation*, **119**(12):1562-1575. [doi:10.1161/Circulationaha.108.804369]

Chauvin, M., Shah, D.C., Haissaguerre, M., Marcellin, L., Brechenmacher, C., 2000. The anatomic basis of connections between the coronary sinus musculature and the left atrium in humans. *Circulation*, **101**(6):647-652. [doi:10.1161/01.CIR.101.6.647]

Cherry, E.M., Evans, S.J., 2008. Properties of two human atrial cell models in tissue: restitution, memory, propagation, and reentry. *J. Theor. Biol.*, **254**(3):674-690. [doi:10.1016/j.jtbi.2008.06.030]

Cherry, E.M., Hastings, H.M., Evans, S.J., 2008. Dynamics of human atrial cell models: restitution, memory, and intracellular calcium dynamics in single cells. *Prog. Biophys. Mol. Biol.*, **98**(1):24-37. [doi:10.1016/j.pbiomolbio.2008.05.002]

Cosio, F.G., Martin-Penato, A., Pastor, A., Nunez, A., Montero, M.A., Cantale, C.P., Schames, S., 2004. Atrial activation mapping in sinus rhythm in the clinical electrophysiology laboratory: observations during Bachmann's bundle block. *J. Cardiovasc. Electrophysiol.*, **15**(5):524-531. [doi:10.1046/j.1540-8167.2004.03403.x]

Courtemanche, M., Ramirez, R.J., Nattel, S., 1998. Ionic mechanisms underlying human atrial action potential properties: insights from a mathematical model. *Am. J. Physiol.*, **44**(1):H301-H321.

de Ponti, R., Ho, S.Y., Salerno-Uriarte, J.A., Tritto, M., Spadacini, G., 2002. Electroanatomic analysis of sinus impulse propagation in normal human atria. *J. Cardiovasc. Electrophysiol.*, **13**(1):1-10. [doi:10.1046/j.1540-8167.2002.00001.x]

Deng, D.D., Xia, L., 2010. Study the Effect of Tissue Heterogeneity and Anisotropy in Atrial Fibrillation Based on a Human Atrial Model. Computing in Cardiology, p.433-436.

Deng, D., Jiao, P., Shou, G., Xia, L., 2009. Registering Myocardial Fiber Orientations with Heart Geometry Using Iterative Closest Points Algorithms. Medical Imaging, Parallel Processing of Images, and Optimization Techniques. Proc. SPIE, Yichang, China, p.74972P-74974P. [doi:10.1117/12.830695]

Deng, D., Jiao, P., Ye, X., Xia, L., 2012. An image-based model of the whole human heart with detailed anatomical structure and fiber orientation. *Comput. Math. Methods Med.*, **2012**:16. [doi:10.1155/2012/891070]

Dolber, P.C., Spach, M.S., 1989. Structure of canine Bachmann's bundle related to propagation of excitation. *Am. J. Physiol.*, **257**(5 Pt 2):H1446-H1457.

Duytschaever, M., Danse, P., Eysbouts, S., Allessie, M., 2002. Is there an optimal pacing site to prevent atrial fibrillation? An experimental study in the chronically instrumented goat. *J. Cardiovasc. Electrophysiol.*, **13**(12):1264-1271. [doi:10.1046/j.1540-8167.2002.01264.x]

Everett, T.H.T., Wilson, E.E., Verheule, S., Guerra, J.M., Foreman, S., Olgin, J.E., 2006. Structural atrial remodeling alters the substrate and spatiotemporal organization of atrial fibrillation: a comparison in canine models of structural and electrical atrial remodeling. *Am. J. Physiol.*, **291**(6):H2911-H2923. [doi:10.1152/ajpheart.01128.2005]

Fedorov, V.V., Glukhov, A.V., Chang, R., Kostecki, G., Aferol, H., Hucker, W.J., Wuskell, J.P., Loew, L.M., Schuessler, R.B., Moazami, N., *et al.*, 2010. Optical mapping of the isolated coronary-perfused human sinus node. *J. Am. Coll. Cardiol.*, **56**(17):1386-1394. [doi:10.1016/j.jacc.2010.03.098]

Feng, J.L., Yue, L.X., Wang, Z.G., Nattel, S., 1998. Ionic mechanisms of regional action potential heterogeneity in the canine right atrium. *Circ. Res.*, **83**(5):541-551. [doi:10.1161/01.RES.83.5.541]

Gray, R.A., Pertsov, A.M., Jalife, J., 1996. Incomplete reentry and epicardial breakthrough patterns during atrial fibrillation in the sheep heart. *Circulation*, **94**(10):2649-2661. [doi:10.1161/01.CIR.94.10.2649]

Hansson, A., Holm, M., Blomstrom, P., Johansson, R., Luhrs, C., Brandt, J., Olsson, S.B., 1998. Right atrial free wall conduction velocity and degree of anisotropy in patients with stable sinus rhythm studied during open heart surgery. *Eur. Heart J.*, **19**(2):293-300. [doi:10.1053/euhj.1997.0742]

Harrild, D., Henriquez, C., 2000. A computer model of normal conduction in the human atria. *Circ. Res.*, **87**(7):E25-E36. [doi:10.1161/01.RES.87.7.e25]

Hayashi, H., Lux, R.L., Wyatt, R.F., Burgess, M.J., Abildskov, J.A., 1982. Relation of canine atrial activation sequence

to anatomic landmarks. *Am. J. Physiol.*, **242**(3): H421-H428.

Henriquez, C.S., Muzikant, A.L., Smoak, C.K., 1996. Anisotropy, fiber curvature, and bath loading effects on activation in thin and thick cardiac tissue preparations: simulations in a three-dimensional bidomain model. *J. Cardiovasc. Electrophysiol.*, **7**(5):424-444. [doi:10.1111/j.1540-8167.1996.tb00548.x]

Ho, S.Y., Sanchez-Quintana, D., 2009. The importance of atrial structure and fibers. *Clin. Anat.*, **22**(1):52-63. [doi:10.1002/Ca.20634]

Ho, S.Y., Sanchez-Quintana, D., Cabrera, J.A., Anderson, R.H., 1999. Anatomy of the left atrium: implications for radiofrequency ablation of atrial fibrillation. *J. Cardiovasc. Electrophysiol.*, **10**(11):1525-1533. [doi:10.1111/j.1540-8167.1999.tb00211.x]

Ho, S.Y., Anderson, R.H., Sanchez-Quintana, D., 2002a. Atrial structure and fibres: morphologic bases of atrial conduction. *Cardiovasc. Res.*, **54**(2):325-336. [doi:10.1016/S0008-6363(02)00226-2]

Ho, S.Y., Anderson, R.H., Sanchez-Quintana, D., 2002b. Gross structure of the atriums: more than an anatomic curiosity? *Pacing Clin. Electrophysiol.*, **25**(3):342-350. [doi:10.1046/j.1460-9592.2002.00342.x]

Hucker, W.J., Mccain, M.L., Laughner, J.I., Iaizz, P.A., Efimov, I.R., 2008. Connexin 43 expression delineates two discrete pathways in the human atrioventricular junction. *Anat. Rec.*, **291**(2):204-215. [doi:10.1002/Ar.20631]

Jacquemet, V., Virag, N., Ihara, Z., Dang, L., Blanc, O., Zozor, S., Vesin, J.M., Kappenberger, L., Henriquez, C., 2003. Study of unipolar electrogram morphology in a computer model of atrial fibrillation. *J. Cardiovasc. Electrophysiol.*, **14**(10):S172-S179. [doi:10.1046/j.1540.8167.90308.x]

James, T.N., 2002. Structure and function of the sinus node, AV node and his bundle of the human heart: Part I—structure. *Prog. Cardiovasc. Dis.*, **45**(3):235-267. [doi:10.1053/pcad.2002.130388]

Jurkko, R., 2009. Atrial Electric Signal During Sinus Rhythm in Lone Paroxysmal Atrial Fibrillation. PhD Thesis, Helsinki University Central Hospital, Helsinki, p.1-108.

Jurkko, R., Mantynen, V., Tapanainen, J.M., Montonen, J., Vaananen, H., Parikka, H., Toivonen, L., 2009. Non-invasive detection of conduction pathways to left atrium using magnetocardiography: validation by intra-cardiac electroanatomic mapping. *Europace*, **11**(2): 169-177. [doi:10.1093/europace/eun335]

Jurkko, R., Mantynen, V., Lehto, M., Tapanainen, J.M., Montonen, J., Parikka, H., Toivonen, L., 2010. Interatrial conduction in patients with paroxysmal atrial fibrillation and in healthy subjects. *Int. J. Cardiol.*, **145**(3):455-460. [doi:10.1016/j.ijcard.2009.05.064]

Kamkin, A., Kiseleva, I., Isenberg, G., Wagner, K.D., Gunther, J., Theres, H., Scholz, H., 2003. Cardiac fibroblasts and the mechano-electric feedback mechanism in healthy and diseased hearts. *Prog. Biophys. Mol. Biol.*, **82**(1-3): 111-120.

Khaja, A., Flaker, G., 2005. Bachmann's bundle: does it play a role in atrial fibrillation? *Pacing Clin. Electrophysiol.*, **28**(8):855-863. [doi:10.1111/j.1540-8159.2005.00168.x]

Kojodjojo, P., Kanagaratnam, P., Markides, V., Davies, W., Peters, N., 2006. Age-related changes in human left and right atrial conduction. *J. Cardiovasc. Electrophysiol.*, **17**(2):120-127. [doi:10.1111/j.1540-8167.2006.00293.x]

Koura, T., Hara, M., Takeuchi, S., Ota, K., Okada, Y., Miyoshi, S., Watanabe, A., Shiraiwa, K., Mitamura, H., Kodama, I., *et al*., 2002. Anisotropic conduction properties in canine atria analyzed by high-resolution optical mapping: preferential direction of conduction block changes from longitudinal to transverse with increasing age. *Circulation*, **105**(17):2092-2098. [doi:10.1161/01.CIR.0000015506.36371.0D]

Lemery, R., Guiraudon, G., Veinot, J.P., 2003. Anatomic description of Bachmann's bundle and its relation to the atrial septum. *Am. J. Cardiol.*, **91**(12):1482-1485. [doi:10.1016/S0002-9149(03)00405-3]

Lemery, R., Soucie, L., Martin, B., Tang, A.S.L., Green, M., Healey, J., 2004. Human study of biatrial electrical coupling-determinants of endocardial septal activation and conduction over interatrial connections. *Circulation*, **110**(15):2083-2089. [doi:10.1161/01.Cir.0000144461.83835.A1]

Lemery, R., Birnie, D., Tang, A.S., Green, M., Gollob, M., Hendry, M., Lau, E., 2007. Normal atrial activation and voltage during sinus rhythm in the human heart: an endocardial and epicardial mapping study in patients with a history of atrial fibrillation. *J. Cardiovasc. Electrophysiol.*, **18**(4):402-408. [doi:10.1111/j.1540-8167.2007.00762.x]

Lorange, M., Gulrajani, R.M., 1993. A computer heart model incorporating anisotropic propagation. I. Model construction and simulation of normal activation. *J. Electrocardiol.*, **26**(4):245-261. [doi:10.1016/0022-0736(93)90047-H]

Lu, W.X., Xu, Z.Y., Fu, Y.J., 1993. Microcomputer-based cardiac field simulation-model. *Med. Biol. Eng. Comput.*, **31**(4):384-387. [doi:10.1007/BF02446692]

Maleckar, M.M., Greenstein, J.L., Giles, W.R., Trayanova, N.A., 2009. K^+ current changes account for the rate dependence of the action potential in the human atrial myocyte. *Am. J. Physiol. Heart Circ. Physiol.*, **297**(4): H1398-H1410. [doi:10.1152/ajpheart.00411.2009]

Markides, V., Schilling, R.J., Ho, S.Y., Chow, A.W., Davies, D.W., Peters, N.S., 2003. Characterization of left atrial activation in the intact human heart. *Circulation*, **107**(5):733-739. [doi:10.1161/01.CIR.0000048140.31785.02]

Matsuyama, T., Ishibashi-Ueda, H., Ikeda, Y., Yamada, Y., Okamura, H., Noda, T., Satomi, K., Suyama, K., Shimizu, W., Aihara, N., *et al*., 2010. The positional relationship between the coronary sinus musculature and the atrioventricular septal junction. *Europace*, **12**(5):719-725. [doi:10.1093/europace/euq067]

Nygren, A., Fiset, C., Firek, L., Clark, J.W., Lindblad, D.S., Clark, R.B., Giles, W.R., 1998. Mathematical model of an

adult human atrial cell-the role of K^+ currents in repolarization. *Circ. Res.*, **82**(1):63-81. [doi:10.1161/01.RES.82.1.63]

Rijcken, J., Bovendeerd, P.H.M., Schoofs, A.J.G., van Campen, D.H., Arts, T., 1999. Optimization of cardiac fiber orientation for homogeneous fiber strain during ejection. *Ann. Biomed. Eng.*, **27**(3):289-297. [doi:10.1114/1.147]

Rohmer, D., Sitek, A., Gullberg, G.T., 2007. Reconstruction and visualization of fiber and laminar structure in the normal human heart from ex vivo diffusion tensor magnetic resonance imaging (DTMRI) data. *Invest. Radiol.*, **42**(11):777-789. [doi:10.1097/RLI.0b013e3181238330]

Roithinger, F.X., Cheng, J., Sippensgroenewegen, A., Lee, R.J., Saxon, L.A., Scheinman, M.M., Lesh, M.D., 1999. Use of electroanatomic mapping to delineate transseptal atrial conduction in humans. *Circulation*, **100**(17):1791-1797. [doi:10.1161/01.CIR.100.17.1791]

Sachse, F.B., Werner, C.D., Stenroos, M.H., Schulte, R.F., Zerfass, P., Dössel, O., 2000. Modeling the Anatomy of the Human Heart Using the Cryosection Images of the Visible Female Dataset. Proc. 3rd Users Conference of the National Library of Medicine's Visible Human Project. Bethesda, USA.

Sanchez-Quintana, D., Anderson, R.H., Cabrera, J.A., Climent, V., Martin, R., Farre, J., Ho, S.Y., 2002. The terminal crest: morphological features relevant to electrophysiology. *Heart*, **88**(4):406-411. [doi:10.1136/heart.88.4.406]

Saremi, F., Channual, S., Krishnan, S., Gurudevan, S.V., Narula, J., Abolhoda, A., 2008. Bachmann bundle and its arterial supply: imaging with multidetector CT—implications for interatrial conduction abnormalities and arrhythmias. *Radiology*, **248**(2):447-457. [doi:10.1148/radiol.2482071908]

Seemann, G., Hoper, C., Sachse, F.B., Dossel, O., Holden, A.V., Zhang, H., 2006. Heterogeneous three-dimensional anatomical and electrophysiological model of human atria. *Philos. Transact. A: Math Phys. Eng. Sci.*, **364**(1843):1465-1481. [doi:10.1098/rsta.2006.1781]

Sun, H., Khoury, D.S., 2001. Electrical conduits within the inferior atrial region exhibit preferential roles in interatrial activation. *J. Electrocardiol.*, **34**(1):1-14. [doi:10.1054/jelc.2001.22065]

Tanaka, K., Zlochiver, S., Vikstrom, K.L., Yamazaki, M., Moreno, J., Klos, M., Zaitsev, A.V., Vaidyanathan, R., Auerbach, D.S., Landas, S., *et al.*, 2007. Spatial distribution of fibrosis governs fibrillation wave dynamics in the posterior left atrium during heart failure. *Circ. Res.*, **101**(8):839-847. [doi:10.1161/CIRCRESAHA.107.153858]

Tapanainen, J.M., Jurkko, R., Holmqvist, F., Husser, D., Kongstad, O., Makijarvi, M., Toivonen, L., Platonov, P.G., 2009. Interatrial right-to-left conduction in patients with paroxysmal atrial fibrillation. *J. Interv. Card. Electrophysiol.*, **25**(2):117-122. [doi:10.1007/s10840-008-9359-2]

Tellez, J.O., Dobrzynski, H., Greener, I.D., Graham, G.M., Laing, E., Honjo, H., Hubbard, S.J., Boyett, M.R., Billeter, R., 2006. Differential expression of ion channel transcripts in atrial muscle and sinoatrial node in rabbit. *Circ. Res.*, **99**(12):1384-1393. [doi:10.1161/01.RES.0000251717.98379.69]

ten Tusscher, K.H.W.J., Noble, D., Noble, P.J., Panfilov, A.V., 2004. A model for human ventricular tissue. *Am. J. Physiol. Heart Circ. Physiol.*, **286**(4):H1573-H1589. [doi:10.1152/ajpheart.00794.2003]

Wang, K., Ho, S.Y., Gibson, D.G., Anderson, R.H., 1995. Architecture of atrial musculature in humans. *Br. Heart J.*, **73**(6):559-565. [doi:10.1136/hrt.73.6.559]

Whiteley, J.P., 2006. An efficient numerical technique for the solution of the monodomain and bidomain equations. *IEEE Trans. Biomed. Eng.*, **53**(11):2139-2147. [doi:10.1109/Tbme:2006.879425]

Wu, T.J., Yashima, M., Xie, F., Athill, C.A., Kim, Y.H., Fishbein, M.C., Qu, Z., Garfinkel, A., Weiss, J.N., Karagueuzian, H.S., *et al.*, 1998. Role of pectinate muscle bundles in the generation and maintenance of intra-atrial reentry: potential implications for the mechanism of conversion between atrial fibrillation and atrial flutter. *Circ. Res.*, **83**(4):448-462. [doi:10.1161/01.RES.83.4.448]

Zhang, H., Holden, A.V., Kodama, I., Honjo, H., Lei, M., Varghese, T., Boyett, M.R., 2000. Mathematical models of action potentials in the periphery and center of the rabbit sinoatrial node. *Am. J. Physiol. Heart Circ. Physiol.*, **279**(1):H397-H421.

Zozor, S., Blanc, O., Jacquemet, V., Virag, N., Vesin, J.M., Pruvot, E., Kappenberger, L., Henriquez, C., 2003. A numerical scheme for modeling wavefront propagation on a monolayer of arbitrary geometry. *IEEE Trans. Biomed. Eng.*, **50**(4):412-420. [doi:10.1109/TBME.2003.809505]